Homogenization in non-linear dynamics due to frictional contact

G. Peillex, Laurent Baillet, Yves Berthier

Homogenization in non linear dynamics due to frictional contact

Peillex G. [a], Baillet L. [b], Berthier Y. [a]

[a]*LaMCoS, INSA-Lyon, CNRS UMR5259, F69621, France*
[b]*LGIT, CNRS - UJF, Maison des Géosciences-38400 Saint-Martin-D'Hères, FRANCE*

Abstract

This work is devoted to a study of the classical homogenization process and its influence on the behavior of a composite under non linear dynamic loading due to contact and friction. Firstly, the general problem of convergence of numerical models subjected to dynamic contact with friction loading is addressed. The use of a regularized friction law allows obtaining good convergence of such models. This study shows that for a dynamic contact with friction loading, the classical homogenization process, coupled with an homogenization of the frictional contact, enables replacing the entire heterogeneous model by a homogenized one. The dynamic part of the frictional contact must be homogenized by modifying the dynamic parameter of the friction law. Modification of the dynamic parameter of the friction law is function of the type and regime of instability. A calculation of a homogenized friction coefficient is presented in view to homogenizing the static part of the frictional contact when the friction coefficient is not constant over the contact surface. Finally matrix and heterogeneities stresses in the heterogeneous models are identified by using the relocalization process and a frictional contact dynamic analysis of a homogeneous model. *To cite this article: Peillex G., Baillet L., Berthier Y., International Journal of Solids and Structures (2008).*

Résumé

Key words: Homogenization ; localization ; non-linear dynamic ; contact ; friction ; finite elements

1. INTRODUCTION

The subject of composite materials under frictional contact loading is of great interest to the aeronautical industry. However frictional contact is a complex form of non linear dynamical loading. The main characteristics of such loading are caused by instabilities at the contact interface. This fact has been widely studied for homogeneous materials (Adams, 1995)(Oueslati et al., 2003)(Linck, 2005)(Massi et al. 2007). From a numerical point of view, frictional contact loading with a constant Coulomb friction coefficient may be ill posed (Martins and Simões, 1998)(Ranjith and Rice, 2001)(Renardy, 1992) and so convergence of numerical models may be hard to achieve. However, experimental studies (Prakash 1993)(Prakash and Clifton, 2001), have led to the formulation of a specific friction law called the "Prakash Clifton" law. It appears that a simplified version of this law avoids ill-posed situations in numerical frictional contact problems (Cochard and Rice, 2000). All the studies cited above were carried out with homogeneous and mostly isotropic materials. Alart and Lebon (1998) mixed static frictional contact and heterogeneous materials. To our knowledge no work on

---

Email address: `guillaume.peillex@insa-lyon.fr` (Peillex G.).

homogenization under dynamic contact with friction loading has been published as yet. This work is devoted to the study of a composite under non linear dynamic loading. Contact with friction boundary conditions leads to considerable non linearity. The two different scales of the composite are studied. A comparison is drawn between the results obtained from heterogeneous models (matrix+heterogeneities) that represent the mesoscopic scale of the material, and from a homogeneous model representing the macroscopic scale whose properties are obtained by using classical homogenization theory (Bornert et al., 2001). Although the different heterogeneous models all have the same homogenized stiffness matrix, which will be that of the homogeneous model, it will be shown that for certain loading cases the heterogeneous models do not exhibit the same behavior under dynamic frictional contact loading.

The following study is divided into three parts. The first introduces the numerical model, the particular friction law, achieving convergence and the specificities of the material. The second is devoted to mapping from mesoscopic to macroscopic scale by applying the homogenization procedure to the elastic properties of the heterogeneous model and by homogenizing the frictional contact. Particular attention is given to the role of the different parameters of the friction law and to the determination of the values of these parameters entered in the homogeneous model. The aim of the previous determination was to ensure that the homogeneous model exhibited the same frictional contact behavior as the heterogeneous ones. The last part is a reversal of the second part as it deals with macro to meso mapping with relocalization procedures. This process, introduced by Kruch et al. (Kruch and Forest, 1998)(Kruch et al., 2004), for the quasi-static loading of composite materials, is used to obtain the stresses at the mesoscopic scale of the material (heterogeneous models) by performing simulations of the macroscopic scale. This part will emphasize the ability of this process under dynamic frictional contact loading.

2. NUMERICAL MODEL

2.1. *Finite element formulation*

The problem of unilateral contact with Coulomb friction problem (cf. figure 1) consists in finding the displacement u and the second order stress tensor $\underline{\sigma}(u)$ satisfying the equation (1) of the mechanics, unilateral contact (2), and Coulomb friction law (3) :

$$\begin{cases} \underline{\sigma}(u) = \underline{\underline{D}}\,\underline{\epsilon}(u) \ \text{ in } \Omega_1 \\ \mathbf{div}\underline{\sigma}(u) + \boldsymbol{f} = \rho\ddot{\boldsymbol{u}} \ \text{ in } \Omega_1 \\ \underline{\sigma}(u)\underline{n} = \underline{P} \quad \text{over } \Gamma_2 \\ \boldsymbol{u}.\boldsymbol{t} = 0 \ \text{ over } \Gamma_2 \end{cases} \tag{1}$$

$$[\boldsymbol{u}.\boldsymbol{n}] \leq 0, \quad \sigma_n(u) \leq 0, \quad \sigma_n(u)\,[\boldsymbol{u}.\boldsymbol{n}] = 0 \ \text{ over } \Gamma_4 \tag{2}$$

$$\begin{cases} |\sigma_t| < \mu\,|\sigma_n| \Rightarrow \text{stick: } [\dot{u}] = 0 \\ |\sigma_t| = \mu\,|\sigma_n| \Rightarrow \text{slip: } \exists \gamma \geq 0 \quad \text{s.t.} \quad [\dot{u}] = -\gamma\sigma_t \end{cases} \tag{3}$$

where ρ is the density, $\underline{\underline{D}}$ is the fourth order tensor of the linear elasticity, $\underline{\epsilon}(u) = (\nabla(u) + \nabla(u)^T)/2$ is the linearized strain tensor, σ_n and σ_t is the normal and tangential contact stress acting on the surface Γ_4, $\boldsymbol{f}$ is the external forces distribution acting on the pin, $\underline{P}$ is the applied pressure, n and t stand for the normal and tangential directions for the surface considered while $[x]$ is the symbol for the jump of variable x at the contact interface Γ_4. The double dot superscript stands for the second partial derivative relative to time.

As the simulations take into account non linear dynamic effects, the PlastD (Baillet and Sassi, 2002)(Linck et al., 2003) 2D explicit dynamic finite element laboratory code is employed to solve the systems (1), (2) and (3). This software uses the forward Lagrange multiplier (4) method to determine the contact forces, λ_n, and a Newmark-β_2 time integration scheme (Bathe, 1982)(Hughes, 1987) (5).
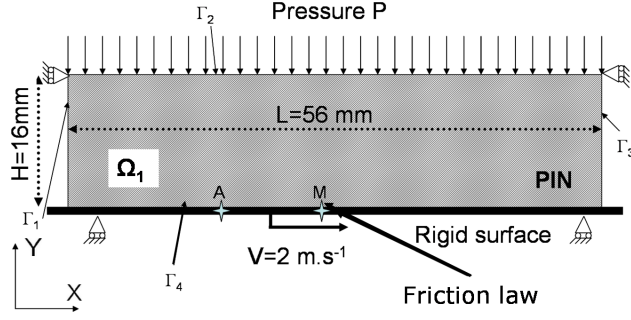
Figure 1. Boundary conditions and the model used.

The equation of the forward increment Lagrange multiplier method is constructed using equations of motion developed via the principle of a virtual work equation at time t_n ($t_n = n\Delta t$) and the displacement constraints acting on the surfaces in contact at time t_{n+1}

$$\begin{cases} \mathbb{M}\ddot{\boldsymbol{u}}_n + \mathbb{C}\dot{\boldsymbol{u}}_n + \mathbb{K}\boldsymbol{u}_n + \mathbb{G}_{n+1}^T \boldsymbol{\lambda}_n = \boldsymbol{f}_n^{ext} \\ \mathbb{G}_{n+1}\left\{\boldsymbol{x}_n + \boldsymbol{u}_{n+1} - \boldsymbol{u}_n\right\} \leq 0 \\ \mathbb{C} = \beta\mathbb{K} \end{cases} \qquad (4)$$

where $\mathbb{G}_{n+1}$ is the global matrix of the constraint, $\boldsymbol{u}_n$ and $\boldsymbol{u}_{n+1}$ are the displacement vectors at time t_n and t_{n+1}, $\boldsymbol{x}_n$ and $\boldsymbol{x}_{n+1}$ are the position vectors respectively at time t_n and t_{n+1}. $\mathbb{M}$, $\mathbb{C}$ and $\mathbb{K}$ are respectively the mass , damping and stiffness matrices. β is a damping coefficient. $\boldsymbol{f}_n^{ext}$ are the nodal vectors of external forces. The dot and double dot superscript stand for first and second partial derivative related to time. At any time step, the velocity $\dot{\boldsymbol{u}}_n$ and acceleration $\ddot{\boldsymbol{u}}_n$ vectors are related to displacements and time step Δt in accordance with the β_2 method ($\beta_2 \in [0.5; 1[$)

$$\begin{cases} \dot{\boldsymbol{u}}_n = \frac{1}{1+2\beta_2}\left[\dot{\boldsymbol{u}}_{n-1} + \Delta t(1-\beta_2)\ddot{\boldsymbol{u}}_{n-1} + \frac{2\beta_2}{\Delta t}(\boldsymbol{u}_{n+1} - \boldsymbol{u}_n)\right] \\ \ddot{\boldsymbol{u}}_n = \frac{2}{\Delta t^2}(\boldsymbol{u}_{n+1} - \boldsymbol{u}_n - \Delta t\dot{\boldsymbol{u}}_n) \end{cases} \qquad (5)$$

In order to achieve stability and convergence of the β_2 method, the time increment Δt must conform to the Courant-Friedrichs-Lewy condition (Sanz-Serna and Spijker, 1986) :

$$\Delta t \leq \frac{h_{mini}}{c_L} \qquad (6)$$

where h_{mini} is the minimal element length and c_L is the longitudinal wave velocity of the material. The time step Δt is equal to $5ns$ throughout this study. The element length used in this study, $h_{mini} = 10^{-4}m$, is much smaller than the wavelength $\lambda = \frac{c}{f}$ of the frequencies, f, which arise in the model ($\approx 10^5 Hz$)(figure 5(c)). For $c_L = 4400ms^{-1}$ and $f \leq 10^5 Hz$, λ is estimated at $440.10^{-4}m$ which is much larger than the element size.

The deformable/rigid model used is shown in figure 1. It consists of a rectangular pin (Ω_1), modeled with linear quadrilateral finite elements assumed to be under plane strain, rubbing against a rigid flat surface with a translation velocity of $2m.s^{-1}$.A pressure P is applied on the top of the pin. The status of a node on the contact surface is obtained by using a friction law (3). The loading due to dynamic contact with a constant friction coefficient is neither uniform over the whole model nor constant. Contact instabilities coexisting with the waves can occur and propagate in the model and are observed experimentally (Ben-Zion, 2001)(Lykotrafitis and Rosakis, 2004)(Xia et al., 2004). These instabilities are of different types depending on the different contact statuses (stick, slip or separated) that occur in the model. The works of Linck (Linck et al., 2003), Oueslati (Oueslati et al., 2003), Adams (Adams, 1995) and Martins (Martins et al., 1999) show that, due to the non linearity of the problem, the type of instabilities depends on the elastic properties of the material and on the applied pressure - velocity pair of the rigid flat surface.

In order to avoid convergence problems that can occur when using a classical Coulomb law (3), a regularized Coulomb friction law, also called simplified "Prakash-Clifton" law (7), is used (Peillex et al., 2006) to model

solids rubbing against one each other numerically (Ranjith and Rice, 2001)(Cochard and Rice, 2000). This regularized friction law (figure 2) links the tangential contact stress σ_t to the normal contact stress σ_n by way of the friction coefficient μ

$$\begin{cases} |\sigma_t^*| < \mu\,|\sigma_n| \Rightarrow \text{stick: } [\dot{u}] = 0; \sigma_t = \sigma_t^* \\ |\sigma_t^*| > \mu\,|\sigma_n| \Rightarrow \begin{cases} \text{slip: } \dot{\sigma}_t = -\,|V|\,/L^*(\sigma_t - \alpha\mu\,|\sigma_n|) \\ \exists\gamma \geq 0 \quad \text{s.t.} \quad [\dot{u}] = -\gamma\sigma_t \end{cases} \qquad \alpha = \begin{cases} 1 & \sigma_t^* \geq 0 \\ -1 & \sigma_t^* < 0. \end{cases} \end{cases} \tag{7}$$

Here $[\dot{u}]$ stands for the relative tangential velocity between a point at the interface and the rigid surface. σ_t^* is the tangential contact stress calculated under the sticking assumption and V is the sliding velocity of the surface. L^* is a length parameter and the superscript dot stands for partial derivative relative to time. Throughout this study the friction coefficient μ is equal to 0.25 at every point of the pin in contact with the rigid flat surface, and if not specified the ratio $\delta = \frac{L^*}{|V|} > 0$ is equal to 300 times the time step ($\Delta t = 5ns$). The friction law used in this study, i.e. the regularized Coulomb friction law, has two parameters: the friction coefficient μ and regularization time δ. The regularized Coulomb friction law tends asymptotically toward the classical Coulomb law. For example, if the normal stress is a Heaviside (figure 2) then the tangential stress follows the same evolution with a classical Coulomb law and for $\mu = 0.25$. With the regularized friction law the response is almost similar except that the step is no longer sharp but has an exponential shape. Figure 2 shows that the friction coefficient μ expresses a slow evolution through time and so is a "static" parameter whereas the regularization time δ expresses the fast evolution of the friction law and so is a "dynamic" parameter.

2.2. *The composite studied*

The model composite (described on figure 1) consists of a collection of heterogeneities embedded in a matrix. The volume rate of the heterogeneities is ten percent. The properties of the matrix and the heterogeneities are summarized in table 1. The heterogeneities are vertical as this is a characteristic of the real composite. They are about a hundred microns in width with a height from 1.2 to 3.6 millimeters (figure 3). The homogeneous model takes the presence of heterogeneities into account by using homogenized properties (10). The aim of this study is to define a homogeneous model that represents the real behavior of the composite under non linear dynamics due to frictional contact. Results concerning convergence are presented first.

2.3. *Convergence of the model and efficiency of the regularized friction law*

The calculations for checking whether convergence is achieved were performed for the slip-separated instability type. The trajectory (figure 4) enhance the separation ($0.2\mu m$) of the node from the rigid flat surface. To summarize the different results regarding convergence obtained with the regularized friction law and for the homogeneous model, figure 5 shows different data concerning the central node in contact, M (figure 1), for models with two different mesh sizes and time steps. All the results except those of figure 5(a) are drawn during the periodic steady state. The phase diagram (figure 5(b)) represents the velocity of a node as a function of its displacement in the same direction (here x) and shows that the periodic steady state is characterized by a limit cycle around an equilibrium position (center of the diagram). The purpose of this figure is therefore to illustrate that the convergence through grid size and time step reduction is achieved. Moreover it provides an idea of the relative tangential velocity and displacement between the contact nodes and the rigid flat surface. This surface has a constant tangential translation speed of $-2000mm.s^{-1}$, whereas the relative tangential speed between the central contact node and the rigid surface evolves between $-1200mm.s^{-1}$ and $-2800mm.s^{-1}$. Figure 5(c) gives an idea of the main frequency ($40kHz$) and of the harmonics ($80kHz$ and $120kHz$) present in the models and shows very good correlation between the two curves representing the two different sets of parameters, once again showing that convergence is achieved. Then figure 5 shows that convergence is achieved even if slip separated contact
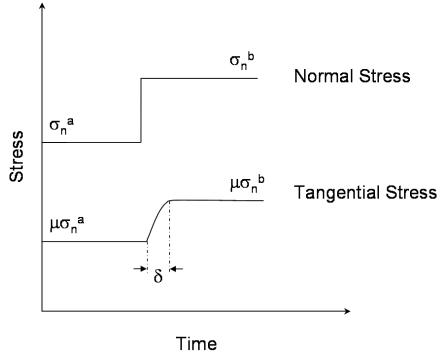
Figure 2. Evolution of the contact tangential stress σ_t with the Prakash-Clifton law after a Heaviside on the contact normal stress σ_n.

	Heterogeneities	Matrix
Young modulus	$E = 240$ GPa	$E = 30$ GPa
Poisson coefficients	$v = 0.2$	$v = 0.2$
Shear modulus	$G = E/2(1+\nu)$	$G = E/2(1+\nu)$
Density	1770 kg/m^3	1770 kg/m^3
Longitudinal wave velocity	$11644 ms^{-1}$	$4116 ms^{-1}$
Shear wave velocity	$7516 ms^{-1}$	$2657 ms^{-1}$

Table 1. Mechanical properties of the components of the composite.
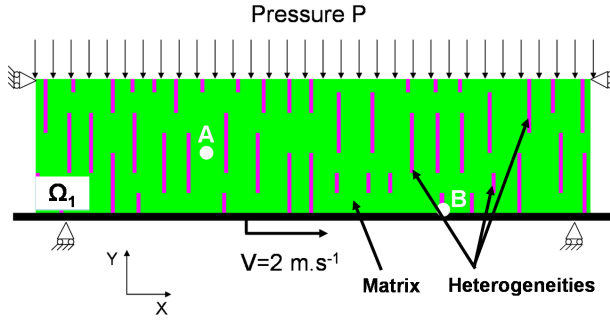

Figure 3. Heterogeneous model : exact morphology (also used for the localization calculations).
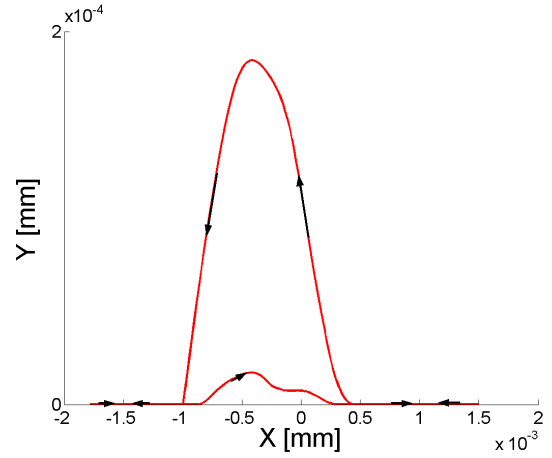

Figure 4. Trajectory of a contact node during the periodic steady state. Slip-separated instabilities ($Y = 0mm$: rigid flat surface).

instabilities exist in the model, as shown here. Moreover, convergence is also achieved for the heterogeneous model although this is not shown here.

2.4. *Particularity of dynamic frictional loading : different instability regimes.*

A crucial issue in the temporal analysis of bodies under dynamic frictional contact is the contact instabilities. These instabilities can be of different types according to the status of the contact nodes. The pressure P applied on the finite element model takes the values $0.4MPa$ or $0.5MPa$. For a friction coefficient μ equal to 0.25 (the same as throughout this study), these two cases correspond to the "slip-separated" contact instability (Linck et al., 2003). An arbitrarily chosen contact node slides on the rigid flat surface or separates from it. For this type of contact instabilities different regimes can appear, depending on the proportion of sliding time of a contact surface node, versus separation time. If an arbitrarily chosen contact node slides 70% of the time and is separated from the rigid surface 30%, it corresponds to regime N°1 ($P = 0.5MPa$). If the same node slides 20% of the time (80% separated), then it will correspond to regime N°2 ($P = 0.4MPa$). A characteristic of the different regimes observed is the apparent friction coefficient $\mu_{app}(t)$. This coefficient is the ratio, at every time step, of the sum of the tangential forces at the upper surface Γ_2 of the model over the sum of the normal forces at the same location. It corresponds to the friction coefficient measured experimentally. The figure 6 presents the evolution through time of the apparent friction coefficient for a
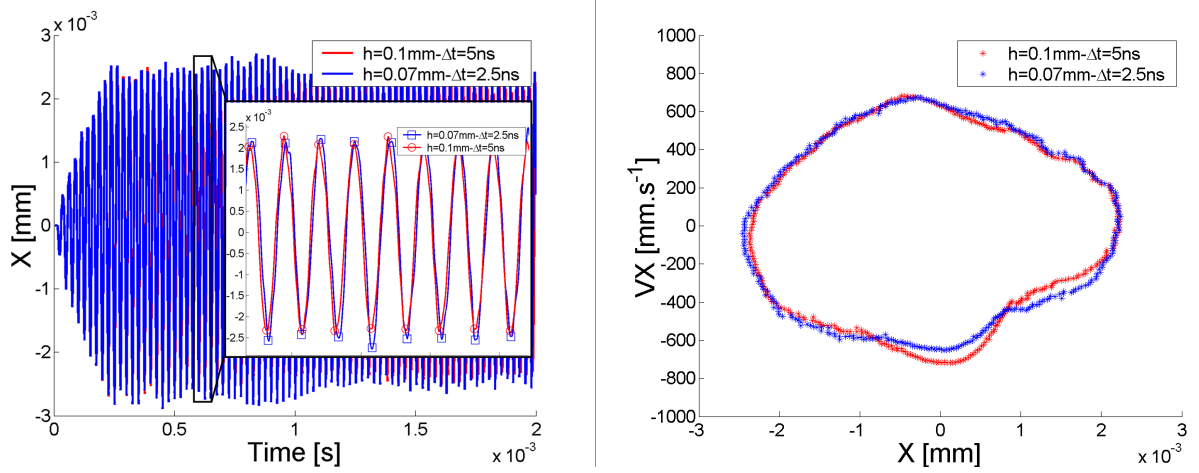
(a) Transient regime $t < 2.5 \times 10^{-4}$ and periodic steady state $t > 2.5 \times 10^{-4}$ of the abscissa.

(b) Mean phase diagram of the tangential movement during the periodic steady state. Limit cycle.
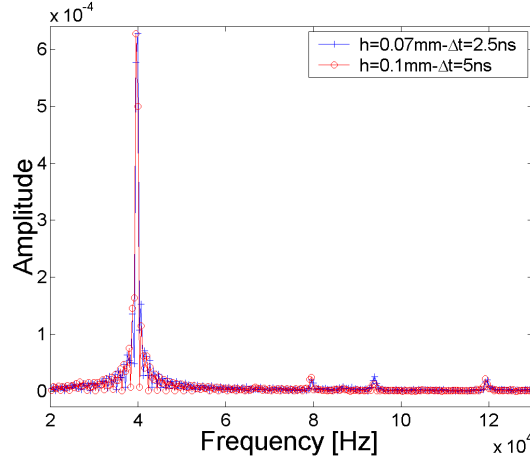
(c) Spectrum of the tangential movement during the periodic steady state.

Figure 5. Different results, concerning the central contact node M (figure 1), illustrating the convergence of the models through grid size ($h = 0.1mm$ and $h = 0.08mm$) and time steps ($\Delta t = 5ns$ and $\Delta t = 2.5ns$) reduction. Convergence is achieved by using to the Coulomb regularized friction law ($\mu = 0.25$, $P = 0.5MPa$, $V = 2ms^{-1}$, $\beta = 4.4e^{-09}$, $\delta = 1500ns$).

homogeneous model under two different loading ($P = 0.5MPa$ and $P = 0.4MPa$) resulting in two different instability regimes. For reasons of readability these types of curves are not be presented in what follows. Instead we use the concept of dissipated frictional energy $E_{friction}$. The dissipated frictional energy is calculated during the simulation, by using the tangential contact force F_t at every contact nodes, and the relative sliding velocity V_{rel} between a contact node and the rigid flat surface :

$$E_{friction} = \int_0^t \sum_{\partial \Omega_{SC}} F_t V_{rel} dt \tag{8}$$

where $\partial \Omega_{SC}$ is the set of the sliding contact nodes.

This dissipated frictional energy can also be related to global quantities of the contact such as the applied pressure P, the velocity of the rigid flat surface V, the whole contact surface S and the global interface friction coefficient μ_{inter}:

$$E_{friction} = \mu_{inter} PSVt \tag{9}$$

6

where t is the time. Figure 7 is analogous with figure 6 but from an energetic point of view. As the periodic steady-state is reached early in the simulation ($t > 2.5 \times 10^{-4}$), the evolution of $E_{friction}$ through time is a straight line. The two regimes dissipate different energies and so are characterized by two different global interface friction coefficients. Due to the presence of instabilities the dissipated frictional energy is less than the one named EPS which would be dissipated if all the contact nodes were sliding at constant speed and if the pressure were uniform. In the following most of the results will be presented by making use of the global interface friction coefficient μ_{inter}.

Remark 1 Although μ_{app} characterizes the friction at the upper surface of the model whereas μ_{inter} describes the friction at the contact surface, the average $\bar{\mu}_{app}$ through time of μ_{app} is equal to μ_{inter}, because from a quasi static point of view the friction force at the upper surface of the model is equal to the one at the contact surface.
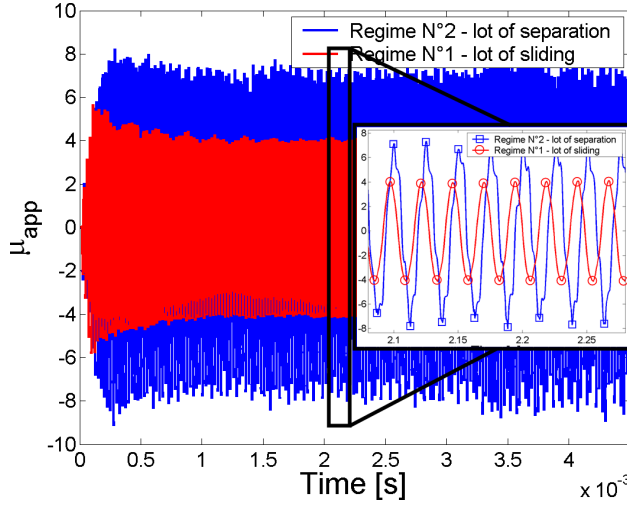

Figure 6. Apparent friction coefficient μ_{app} for two different regimes. The average of this coefficient through time $\bar{\mu}_{app}$ is $\bar{\mu}_{app} = 0.21$ in regime N°1 ($P = 0.5MPa$) and $\bar{\mu}_{app} = 0.17$ in regime N°2 ($P = 0.4MPa$). The main vibration frequency is $f = 41200Hz$ for regime N°1 and is $f = 39600Hz$ for regime N°2.
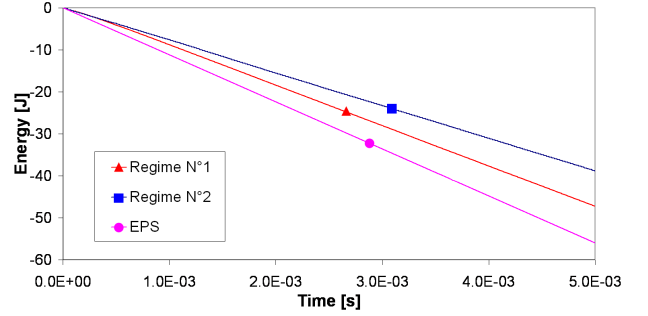
Figure 7. Dissipated frictional contact energy $E_{friction}$ for two different regimes. The slope of this curve in the periodic steady state ($t > 2.5 \times 10^{-4}s$) gives the global interface friction coefficient μ_{inter}. $\mu_{inter} = 0.21$ for regime N°1 ($P = 0.5MPa$) and $\mu_{inter} = 0.17$ for regime N°2 ($P = 0.4MPa$). EPS stands for the energy that would be dissipated if all the contact nodes were sliding at constant speed and if pressure ($P = 0.5MPa$) were uniform. In this case $\mu_{inter} = 0.25 = \mu$.

3. HOMOGENIZATION OF STIFFNESS MATRIX AND ADAPTATION OF THE CONTACT FRICTION LAW

3.1. *Homogenization of the composite material's properties*

In order to determine the homogenized properties of the composite material (table 1), four identical volumes ($\Omega_1 = 16mm \times 56mm$) with four randomized morphologies (i.e randomized distributions of heterogeneities with the same volume fraction : 10%), are modeled in two dimensions with the commercial code Abaqus. The morphologies are assumed to be under plane strains with static loading. As the materials are elastic, the properties are determined by using the classical theory of homogenization. Two different types of boundary conditions (stress or strain homogeneous on the contour $\Gamma = \Gamma_1 \cup \Gamma_2 \cup \Gamma_3 \cup \Gamma_4$)(figure 1) are applied in order to determine the five constants defining the behavior of a transversely isotropic material (Lemaitre and Chaboche, 2004). It was shown (Bornert et al., 2001)(Kanit et al., 2003) that the results given by these two types of boundary conditions limit the exact result. The very low standard deviation ($\leq 2.7\%$) between the coefficients of the homogenized stiffness matrix obtained with the two types of boundary conditions and for different morphologies proves that the properties shown in matrix $\underline{D}$ (equation 10) are very close to the

7

exact ones and so the volume Ω_1 is sufficiently large to be considered representative of the morphologies, at least under static loading.

$$\underline{\sigma} = \underline{\underline{D}}\underline{\epsilon} \Leftrightarrow \begin{Bmatrix} \sigma_{xx} \\ \sigma_{yy} \\ \sigma_{xy} \end{Bmatrix} = 10^9 . \begin{bmatrix} 36.54 & 9.1 & 0 \\ 9.1 & 47.26 & 0 \\ 0 & 0 & 13.785 \end{bmatrix} \begin{Bmatrix} \epsilon_{xx} \\ \epsilon_{yy} \\ \epsilon_{xy} \end{Bmatrix} (10)$$

3.2. *Homogenization of the stiffness matrix and linear dynamics : a first step before non linear dynamic loading*

The following section deals with a comparison under linear dynamic loading between a homogeneous model, with the properties obtained in the previous section, and a heterogeneous one, defined by heterogeneities embedded in the matrix whose properties are those of table 1. The goal here is to address the question of the scale separation. A crucial issue in the problem of homogenization is the relationship between the size of the heterogeneities and the wavelength of typical elastic waves. If the wavelength of the elastic waves propagating in the model is of the same order of magnitude as the size of the heterogeneities or even smaller, then complex behavior may occur such as dissipation, refraction or diffraction. In such cases it is necessary to use particular homogenization processes capable of taking into account the effect of microstructure on wave propagation (Chen and Fish, 2001)(Fish and Chen, 2004)(Boutin, 1991)(Boutin, 1996)(Boutin and Auriault, 1993). In the cases of dynamic frictional contact loading the main frequency of vibration of the model is about $40kHz$ which correspond to the first vibration mode of the model. Modal analysis with two different boundary conditions (BC1 and BC2) representing two extremal contact cases, figure 8, has shown in the case of the first mode of vibration that the mesostructure has no effect on the dynamic behavior of the model, figures 8(a) and 8(b). It is therefore impossible to dissociate the results given by the heterogeneous model from those of the homogeneous one. This experiment proves that the scale separation is realized for the first mode of vibration. Of course higher frequencies are present in the model, due to the contact instabilities presented below. The spectrum of the normal contact stress reveals that the highest frequency, which has an amplitude higher than 10% of the amplitude of the first frequency, is about $500kHz$. For a longitudinal wave celerity of $c_L = 4400m.s^{-1}$, this frequency correspond to a wavelength $\lambda = 8.8mm$. This wavelength is much higher than the thickness of the heterogeneities ($0.2mm$) and three times higher than the lenght of the heterogeneities ($3mm$). Thus, even if this frequency ($500kHz$) of low amplitude is considered with caution, the corresponding wavelength is much higher than the size of the heterogeneities. Therefore it is possible to conclude that the scale separation is effective, which is why classical homogenization is used in the following.

Heterogeneous model   Homogeneous model

F=40000 Hz   F=40035 Hz

Heterogeneous model   Homogeneous model

F=41580 Hz   F=41586 Hz

(a) Results of the modal analysis for the BC1 boundary condition. (b) Results of the modal analysis for the BC2 boundary condition.
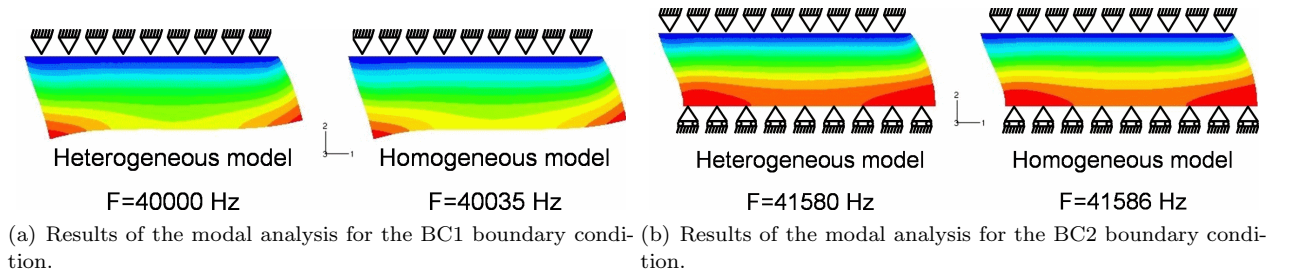
Figure 8. Modal analysis of the model Ω_1.

The frequency ($41580Hz$) obtained by modal analysis when the surface Γ_4 (figure 1) is clamped in the y direction and free along x, i.e. boundary conditions BC2 in figure 8(b), is close to that ($41200Hz$ - figure 6) obtained during a temporal analysis, if the established regime is the first one. Inversely the frequency ($40000Hz$) obtained by modal analysis when the surface Γ_4 (figure 1) is free in directions x and y, boundary

conditions BC1 in figure 8(a), is close to that ($39600Hz$ - figure 6) obtained during a temporal analysis, if the regime established is the second one.

3.3. *Dynamic frictional contact behavior of heterogeneous models*

For each of the loading conditions ($P = 0.5MPa$ and $P = 0.4MPa$) different randomized heterogeneous models with exactly the same friction law ($\mu = 0.25$ and $\delta = 1500ns$) were tested under dynamic frictional contact loading. These models have the particularity of all having the same homogenized stiffness matrix. Thus they are all equivalent under static, and linear dynamic loading. Table 2, which contains the global interface friction coefficient of the four heterogeneous models, shows that for $P = 0.5MPa$, all the heterogeneous models are equivalent, because they dissipate the same frictional energy and so the corresponding global interface coefficients are the same in periodic steady state. All the heterogeneous models are in regime N°1 ($\mu_{inter} \cong 0.215$). Inversely, for $P = 0.4MPa$ this equivalence disappears (table 3). The heterogeneous model N°1 is no more in the regime N°1 but is now in the regime N°2 characterized by $\mu_{inter} = 0.173$ whereas the heterogeneous model N°2 keeps the regime N°1. This difference in the behavior of the heterogeneous models under dynamic frictional loading is probably due to local contact dynamics that are different from one model to the next and thus due to different frictional stresses at the contact interface. This difference of behavior between heterogeneous models with the same homogenized stiffness matrix prevents the homogeneous model from being equivalent to all the heterogeneous models. However, it is shown hereafter that by applying an equation that links contact stress to instability type and regime, it is possible to determine different regularization times δ for incorporation in the homogeneous model to make it equivalent to the heterogeneous models.

3.4. *Considerations about the friction law*

To obtain two equivalent models (heterogeneous and homogeneous) in periodic steady state (i.e. limit cycle), with dynamic friction problem, they must first be equivalent according to the static friction problem. A necessary condition is therefore that they should be subjected to the same tangential static load. Under static loading, the regularization time δ of the friction law does not play any role. This is why the local friction coefficient has to be identical in each model to ensure static equivalence between them.
Another necessary condition to ensure the equivalence of the homogeneous model with the heterogeneous one is that they have the same local contact dynamics (governed by regularization time δ) in order to dissipate the same energy by sliding on the rigid flat surface thus obtain the same global interface friction coefficient.

Therefore to obtain the same local contact dynamics and thus the same global interface friction coefficient, the parameter to be adapted is the regularization time δ. This is the aim of the following section.

3.5. *Influence of regularization time δ on the homogenization process : analytical development*

Here, we focus on a the slip-separated instability regime ($0.15 < \mu < 0.35$). A node of the contact interface slides or impacts on a rigid flat surface. A calculation hypothesis is made in the framework of analytical development. The shape of the real normal contact stress σ_n at node M, figure 9, is approximated by the shape described in figure 10. Thus for period, T, of the signal there is a time, T_G when the normal contact stress is not nil, meaning that the node considered is sliding over the rigid flat surface. T_G depends on the type and on the regime of instability and thus on the different parameters (μ,δ,P,V) that govern the instability type or regime. Time T_G is almost constant for a given regime and type of instability. From equation 7, with the regularization time, δ, the local friction coefficient, μ, and considering that the relative sliding velocity V_{rel} is uniform and constant, then the evolution of the tangential stress for the node considered is

$$\sigma_t = -\mu \, |\sigma_n| \, (1 - e^{\frac{-t}{\delta}}) \frac{V_{rel}}{|V_{rel}|} \tag{11}$$

The friction coefficient $\bar{\mu}$ averaged through time at this node is then equal to

9

$$\bar{\mu} = \frac{1}{T_G} \int_0^{T_G} \mu(1 - e^{\frac{-t}{\delta}}) dt \tag{12}$$

$$\bar{\mu} = \mu[1 + \frac{\delta}{T_G}(e^{-\frac{T_G}{\delta}} - 1)] \tag{13}$$

Consequently, knowledge of the local friction coefficient, μ, the regularization time, δ, and the time of sliding, T_G, makes it possible to estimate the friction coefficient averaged through time $\bar{\mu}$. Thus this particular friction coefficient takes into account the influence of the instabilities. Moreover if we assume that this friction coefficient averaged through time $\bar{\mu}$ is the same over the whole contact, it is possible to link this friction coefficient to the energy dissipated by frictional contact $E_{friction}$:

$$E_{friction} = \bar{\mu}PSVt \tag{14}$$

where P is the pressure applied on surface S and V is the sliding velocity of the rigid surface. Then, with the assumptions made about the shape of the normal stress, $\bar{\mu}$ should be a good approximation of the global interface friction coefficient μ_{inter} (equation 9). In order to validate this fact, a homogeneous model with different regularization time values has been simulated. The global interface friction coefficient obtained from the slope of the frictional dissipated energy curve, μ_{inter} is compared to the friction coefficient averaged through time, $\bar{\mu}$ obtained from equation 13, figure 11. Good correlation is found between the results. The slight difference between the two curves is explained by the fact that analytical calculations are performed with a strong assumption regarding the form of the normal stress (figure 10). The change of sign for the slope for $\delta = 300\Delta t$ is due to the transition from the instability regime N°2 to the N°1. The analytical equation gives good estimations of the global interface friction coefficient and thus of the frictional energy dissipated during contact instabilities.

It is important to note that this estimation requires the calculation of the model (homogeneous or heterogeneous) considered because T_G cannot be determined before the analysis. It is also possible, knowing μ, T_G and the global interface friction coefficient to estimate the regularization time used in the model. It is possible in this way to determine the regularization time needed in the homogeneous model to obtain the same global interface friction coefficient for two models (heterogeneous and homogeneous). A regularization time of the homogeneous model different from that of the heterogeneous model is a way of taking into account the influence of the mesostructure over the behavior of the composite under dynamic with friction loading.

3.6. Homogenization and regularization time

3.6.1. Applied pressure $P = 0.5MPa$

For this applied pressure all the models, both heterogeneous and homogeneous, are in the slip-separated instability type and in the regime N°1. The table 2 shows the global interface friction coefficient for the four heterogeneous model and for the homogeneous model. As it is shown (section 3.3) all the heterogeneous models are equivalent. The analysis of the heterogeneous model and equation 13 made it possible to determine that if $\delta = 1700ns$ the global interface friction coefficient μ_{inter} of the homogeneous model is close to that of the heterogeneous model ($\delta = 1500ns$). The results confirm this determination of δ. There is good equivalence between the results obtained with the homogeneous model $\delta = 1700ns$ and with the heterogeneous ones $\delta = 1500ns$. The analysis of the homogeneous model with $\delta = 1500ns$, revealed that the measured global interface friction coefficient is $\mu_{inter} = 0.22$. For this particular loading case, modifying the regularization time results in slightly better equivalence between the homogeneous model and the heterogeneous one. Other results (not shown here) show that this improvement is important in the transient part of the signal ($t < 2.5 \times 10^{-4}s$).

3.6.2. Applied pressure $P = 0.4MPa$

As described in section 3.3, for this loading case, two heterogeneous models that were equivalent under the previous loading ($P = 0.5MPa$) now have two very different behaviors illustrated by two different global
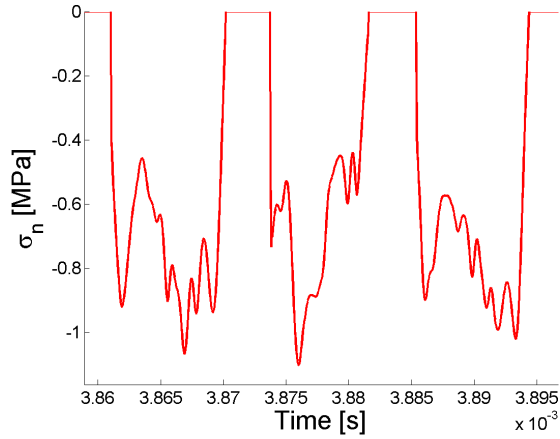
Figure 9. Real evolution of the normal contact stress during slip-separated instability at node M (figure 1) : $\mu = 0.25$, $\delta = 1500ns$, $P = 0.5MPa$, $V = 2ms^{-1}$, $\beta = 4.2 \times 10^{-09}s$.
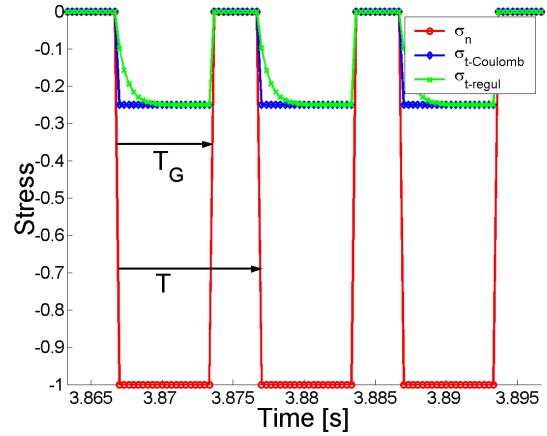
Figure 10. Schematic evolution of tangential stress with the classical Coulomb friction law ($\sigma_{t-Coulomb}$) and with the regularized one ($\sigma_{t-regul}$) when normal contact stress (σ_n) is a succession of steps. The friction coefficient is equal to 0.25.
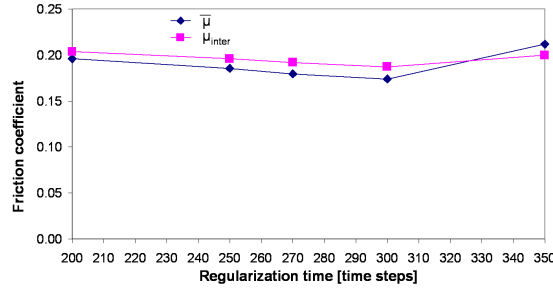

Figure 11. Comparison of the values of the global interface friction coefficient μ_{inter}, obtained by numerical experiments from the slope of the frictional dissipated energy curve, and the friction coefficient $\bar{\mu}$ averaged through time, obtained analytically.

Model and regularization time δ	Global interface friction coefficient μ_{inter}
Heterogeneous N $^{\circ}$ 1 - $\delta = 1500ns$	$\mu_{inter} = 0.215$
Heterogeneous N $^{\circ}$ 2 - $\delta = 1500ns$	$\mu_{inter} = 0.213$
Heterogeneous N $^{\circ}$ 4 - $\delta = 1500ns$	$\mu_{inter} = 0.214$
Heterogeneous N $^{\circ}$ 6 - $\delta = 1500ns$	$\mu_{inter} = 0.216$
Homogeneous - $\delta = 1700ns$	$\mu_{inter} = 0.212$
Homogeneous - $\delta = 1500ns$	$\mu_{inter} = 0.220$

Table 2
Global interface friction coefficient for four heterogeneous models ($\delta = 1500ns$) and for a homogeneous model with two regularization times ($\delta = 1500ns$ and $\delta = 1700ns$). ($\mu = 0.25$, $P = 0.5MPa$, $V = 2m.s^{-1}$)

interface friction coefficients (table 3). Therefore the homogeneous model cannot be simultaneously equal to both heterogeneous models, but the use of equation 13 allows determining that the heterogeneous model called "Heterogeneous N $^{\circ}$ 1" ($\delta = 1500ns$) is equal to the homogeneous model with a regularization time of $\delta = 1500ns$ and that the other heterogeneous model "Heterogeneous N $^{\circ}$ 2" ($\delta = 1500ns$) is equivalent to the homogeneous model with a regularization time of $\delta = 1750ns$. Table 3 confirms these calculations and so proves that thanks to a slight modification of the dynamic parameter (δ) of the friction law it is possible

11

Model and regularization time δ	Global interface friction coefficient μ_{inter}
Heterogeneous N ˚ 1 - $\delta = 1500ns$	$\mu_{inter} = 0.173$
Heterogeneous N ˚ 2 - $\delta = 1500ns$	$\mu_{inter} = 0.213$
Homogeneous - $\delta = 1750ns$	$\mu_{inter} = 0.209$
Homogeneous - $\delta = 1500ns$	$\mu_{inter} = 0.175$

Table 3
Comparison of the effect of the regularization time over the homogenization process. ($P = 0.4MPa$, $V = 2ms^{-1}$).

to obtain equivalence between heterogeneous models and homogeneous ones.

The fact that the two heterogeneous models are no longer equivalent under this loading case has not yet been clearly explained. Image analysis has been performed but no difference between the morphologies of heterogeneous models have been found.

4. HOMOGENIZATION OF THE FRICTION COEFFICIENT

Contrary to the sections above, we now consider the situation in which the friction coefficient at contacts with heterogeneities differs from that at contacts with the matrix. For the heterogeneous model, a particular friction coefficient is attributed to the contact nodes belonging to the heterogeneities (μ_h) and another particular friction coefficient is attributed to the contact nodes belonging to the matrix (μ_m). Only one morphology of the heterogeneous model, with the volume fraction of heterogeneities equal to the surface fraction, is used and compared to the homogeneous model. An analytical development was used to define the value of the homogenized friction coefficient, μ_{homo}, implemented in the analysis of the homogeneous model.

4.1. Homogenization of the friction coefficient: analytical development

The friction coefficient μ_{homo} is obtained by equalizing the frictional power dissipated in the homogeneous model with that dissipated in the heterogeneous ones. As shown in the previous section the friction coefficient expresses the quasi-static evolution of the friction law. Consequently, all the considerations mentioned in this section are based on static considerations and allow the determination of μ_{homo} which is the friction coefficient of the homogeneous model that will ensure that the homogeneous model is equivalent to the heterogeneous ones under static loading. Dynamic equivalence is obtained in a second step by using equation 13 and determining the correct regularization time δ.

In quasi static evolution, the power for the homogeneous model is given by

$$W_{homo} = \mu_{homo}PVS \tag{15}$$

where μ_{homo} is the friction coefficient sought, P the pressure applied on a surface S of the model and V the velocity of the rigid surface. For the heterogeneous model, the total power is equal to the sum of that W_h dissipated through the surface S_h of the heterogeneities and the other one W_m dissipated through the surface S_m of the matrix

$$W_{hetero} = W_h + W_m = \mu_h P_h V S_h + \mu_m P_m V S_m. \tag{16}$$

By equalizing the equations 15 and 16 it is possible to determine the value of μ_{homo} which is the value to be entered in the homogenized model

$$W_{hetero} = W_{homo} \Rightarrow \mu_h P_h S_h + \mu_m P_m S_m = \mu_{homo}PS \tag{17}$$

as the velocity V of translation of the rigid surface is the same in the homogenized and heterogeneous models.

The first way of estimating P_h and P_m is to use the balance equation at the contact interface and the hypothesis of a static pressure distribution (SPR - equation 18). At this contact interface, the assumption is

made that the loading is similar to a strain imposed loading. In such cases the strain of the heterogeneities is equal to that of the matrix :

$$\epsilon_h = \frac{P_h}{E_h} = \epsilon_m = \frac{P_m}{E_m} \tag{18}$$

In this equation E stands for Young's modulus. It allows writing the following equation:

$$\begin{cases} SP = S_h P_h + S_m P_m \\ \text{(SPR hypothesis)} \Leftrightarrow P_h = \frac{P_m E_h}{E_m} \end{cases} \Rightarrow \begin{cases} P_m = \frac{SPE_m}{S_h E_h + S_m E_m} \\ P_h = \frac{SPE_h}{S_h E_h + S_m E_m} \end{cases} \tag{19}$$

Equation 19 gives:

$$\mu_{homo} = \frac{S_h \mu_h E_h + S_m \mu_m E_m}{S_h E_h + S_m E_m} \tag{20}$$

and then, as the surface fraction is equal to the volume fraction :

$$\mu_{homo} = \frac{v_h \mu_h E_h + v_m \mu_m E_m}{v_h E_h + v_m E_m} \tag{21}$$

where v_h and v_m are the volume (or surface) fraction of the heterogeneities and matrices.
Another way of estimating P_h and P_m is to run a static contact analysis (SCA) of the heterogeneous model subjected to a pressure P and to a friction contact. The results given by this process are close to those obtained analytically (table 4). The two processes of calculations of the pressures in the heterogeneities and the matrix give similar homogenized friction coefficients (table 4).

The following subsection is dedicated to the validity of the homogenized friction coefficient calculated.

4.2. *Numerical validation of the homogenization of the friction coefficient*

In this subsection a comparison is made between the results obtained for a couple of local friction co-efficients (μ_h,μ_m), for a heterogeneous model, and the results obtained with the homogenized model with homogenized friction coefficient. The pressure and velocity values of the rigid flat surface are constant: $P = 0.5MPa$, $V = 2ms^{-1}$.

μ_h	μ_m	$P_h SPR$	$P_m SPR$	μ_{homo}	$P_h SCA$	$P_m SCA$	μ_{homo}
0.3	0.12	2.35MPa	0.29MPa	**0.20**	2MPa	0.33MPa	0.19

Table 4
Friction coefficients used in the models. Volume fraction of heterogeneities $v_h = 0.1$, and matrix $v_m = 0.9$. SPR=static pressure repartition ; SCA=static contact analysis.

The couple of local friction coefficients are summarised in table 4. In this table the value of the homogenized friction coefficient is obtained by the formula 17. The value of pressures P_h and P_m are determined by SPR (equation 19) or by a static contact analysis (SCA) of the heterogeneous model. The two methods of calculating the pressures give fairly similar results and the homogeneous friction coefficient μ_{homo} is almost the same for the two methods. The values of the homogeneous friction coefficient used in the numerical calculations are in bold type (table 4).

μ_h=0.3 and μ_m=0.12
Two different results will be presented here. The different global interface friction coefficients are presented in tables whereas the figures show the evolution of the apparent friction coefficient through time during the transient part and during the periodic steady-state.
Table 5 and figure 12 show that the results given by the homogeneous model ($\delta = 1500ns$) are far from that given by the heterogeneous model. An adaptation, provided by equation 13, of the regularization time, δ ($\delta = 2500ns$) considerably improves the quality of the results and thus equivalence is achieved (table 5 and figure 12).

Other couples of friction coefficient have been tested and give the same kind of results.

Remark 2 In the case where $\mu_h = \mu_m$, the tangential stress of contacts under the heterogeneities is higher than that of contacts under the matrix. Then the case where $\mu_h > \mu_m$ is the worst case for the homogenization because it increases this difference of tangential stress. Conversely if $\mu_h < \mu_m$ this difference is slighter.

Model and regularization time δ	Global interface friction coefficient μ_{inter}
Heterogeneous - $\mu_h = 0.3$, $\mu_m = 0.12$, $\delta = 1500ns$	$\mu_{inter} = 0.157$
Homogeneous - $\mu_{homo} = 0.2$, $\delta = 1500ns$	$\mu_{inter} = 0.171$
Homogeneous - $\mu_{homo} = 0.2$, $\delta = 2500ns$	$\mu_{inter} = 0.158$

Table 5
Global interface friction coefficient of the heterogeneous model ($\mu_h = 0.3$, $\mu_m = 0.12$, $\delta = 1500ns$) compared to those given by two homogeneous models ($\mu_{homo} = 0.2$, $\delta = 1500ns$ and $\mu_{homo} = 0.2$, $\delta = 2500ns$).

(a) During the transient part.

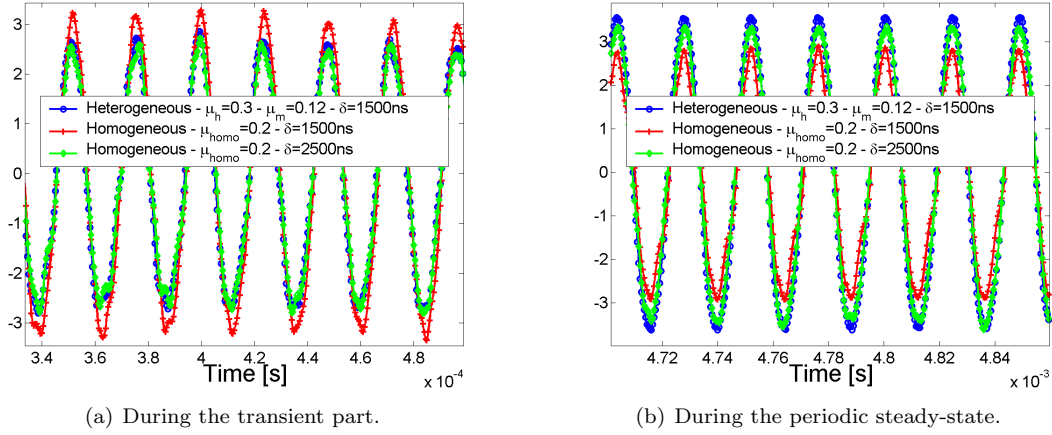(b) During the periodic steady-state.

Figure 12. Apparent friction coefficient for the heterogeneous model ($\mu_h = 0.3$, $\mu_m = 0.12$, $\delta = 1500ns$) compared to those given by two homogeneous models ($\mu_{homo} = 0.2$, $\delta = 1500ns$ and $\mu_{homo} = 0.2$, $\delta = 2500ns$).

Equation 13, can give the same value of $\bar{\mu}$ for two different couples μ-δ. Thus two homogeneous models with two different couples μ-δ can have the same global behavior.

Model and regularization time δ	Global interface friction coefficient μ_{inter}
Heterogeneous - $\mu_h = 0.3$, $\mu_m = 0.12$, $\delta = 1500ns$	$\mu_{inter} = 0.157$
Homogeneous - $\mu_{homo} = 0.23$, $\delta = 1500ns$	$\mu_{inter} = 0.198$
Homogeneous - $\mu_{homo} = 0.23$, $\delta = 4000ns$	$\mu_{inter} = 0.154$

Table 6
Global interface friction coefficient of the heterogeneous model ($\mu_h = 0.3$, $\mu_m = 0.12$, $\delta = 1500ns$) compared to those given by two homogeneous models ($\mu_{homo} = 0.23$, $\delta = 1500ns$ and $\mu_{homo} = 0.23$, $\delta = 4000ns$).

The same homogeneous model with two different couples of local homogenized friction coefficient and regularization time (table 5; $\mu_{homo} = 0.2$; $\delta = 2500ns$) (table 6; $\mu_{homo} = 0.23$; $\delta = 4000ns$) is equivalent to the same heterogeneous model (figure 12 and figure 13). These results are valid for slip-separated contact instabilities ($0.15 < \mu < 0.35$).

4.3. Conclusion

It has been shown in this part that simple equations (17-21) based on static considerations allow determining a homogenized friction coefficient. This homogenized friction coefficient ensures that the quasi-static
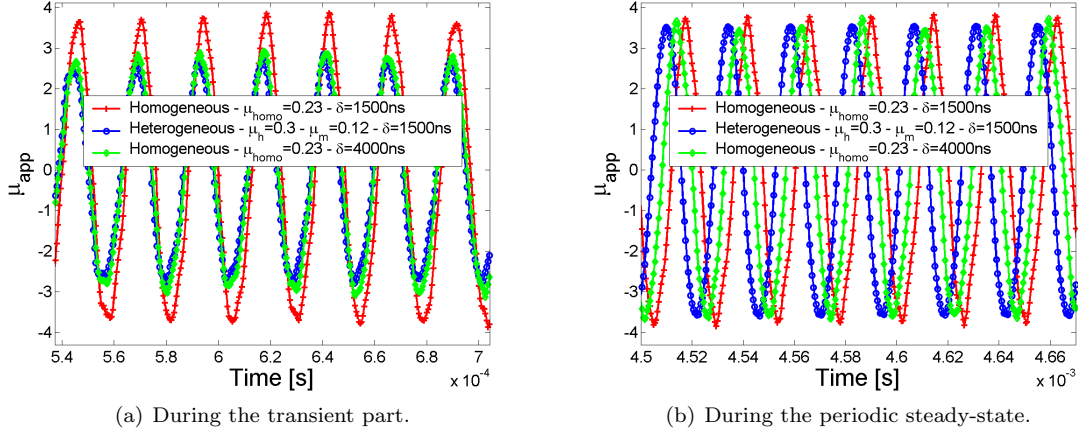
(a) During the transient part. (b) During the periodic steady-state.

Figure 13. Apparent friction coefficient for the heterogeneous model ($\mu_h = 0.3$, $\mu_m = 0.12$, $\delta = 1500ns$) compared to those given by two homogeneous models ($\mu_{homo} = 0.23$, $\delta = 1500ns$ and $\mu_{homo} = 0.23$, $\delta = 4000ns$).

part of the energy received by the homogeneous model is the same as that received by the heterogeneous model. For the dynamic part of the energy it is necessary to determine the regularization time so that the homogeneous model is in the same instability mode (same vibrations frequency) as the heterogeneous model and thus the total energy received by the two models is the same.

Although the equations (17-21) allow determining a homogenized friction predictively, the entire contact homogenization process is not yet totally predictive. In fact determining the required regularization time requires the simulation of the heterogeneous model to determine the instability regime existing within it.

5. LOCALIZATION PROCESS

The previous section focused on mapping from heterogeneous models that represent the mesoscopic scale of the composite to homogeneous ones that represent the macroscopic scale of the material. This section describes the reverse procedure. It focuses on the determination of local stresses in the heterogeneous models, by using the dynamical contact with friction analysis of the homogeneous model.

While performing the calculations to obtain homogenized properties, with homogeneous strain or stress over the contour, it is also possible to determine the localization stress matrix or concentration strain matrix (Bornert et al., 2001). In this study only the strain concentration matrix $\mathbb{L}_x$ is used. The subscript $_x$ means that this concentration matrix $\mathbb{L}_x$ varies in space. For a static loading (subscript $_{stat}$) with homogeneous strain over the contour, it links the local strain vector, $\boldsymbol{\epsilon}_{x_{stat}}$, to the main strain vector over the volume, $\bar{\boldsymbol{\epsilon}}_{stat}$.

$$\begin{cases} \boldsymbol{\epsilon}_{x_{stat}} = \mathbb{L}_x \bar{\boldsymbol{\epsilon}}_{stat} \\ \bar{\boldsymbol{\epsilon}}_{stat} = \frac{1}{V} \int_V \boldsymbol{\epsilon}_{x_{stat}} dv \end{cases} \tag{22}$$

$\mathbb{L}_x$ is determined in a static analysis with homogeneous strain over the contour of heterogeneous models. Classical homogenization theory has shown that this matrix is able to provide the mapping from macroscopic to mesoscopic scale (i.e determine the local stress-strain vectors in the heterogeneities and in the matrix) in a static case subject to the condition that the macroscopic loading is uniform over the volume studied. This section shows that the concentration strain matrix is useful to perform the mapping desired even in the case where, in the model composite (figure 1), loading is dynamic and non uniform over the volume modeled, and if there is contact with friction.

Kruch et al. (2004) have shown that for coarse grain structures the re-localization process is able to perform mapping from macro to meso scale. It consists in applying the concentration (or localization) matrix $\mathbb{L}_x$ to

15

the local strain (or stress) vector of the homogenized model $\boldsymbol{\epsilon}_{xhomo}$ (equation 24) instead of applying it to the mean strain (or stress) vector of the homogenized model $\bar{\boldsymbol{\epsilon}}_{homo}$ (equation 23).

$$\boldsymbol{\epsilon}_{xhetero} = \mathbb{L}_x \bar{\boldsymbol{\epsilon}}_{homo} \tag{23}$$

$$\boldsymbol{\epsilon}_{xhetero} = \mathbb{L}_x \boldsymbol{\epsilon}_{xhomo} \tag{24}$$

The case studied by Kruch et al. is a static one but the macroscopical loading is non uniform over the volume. Moreover the fact that the re-localization process gives such good results is not explained by the theory of homogenization. In the problem studied here, it is the wave propagation in the model and the particular contact conditions which are responsible for non homogeneous macroscopical loading.

This section focuses on the use of the re-localization process to determine the evolution through time of the stress in the heterogeneities and in the matrix. A complete heterogeneous model whose morphology is illustrated in figure 3, is simulated under dynamical contact with friction loading (direct process). The results obtained are those of the reference. The results obtained by the equivalent homogeneous model are modified by the re-localization process. It is possible to obtain the stress in every element of the model by using this process. The results given by the re-localization process and those of reference are compared in figures 14 and 15 for two different elements in the model. The figure 16 shows the Von Mises stress averaged through time over the whole model.
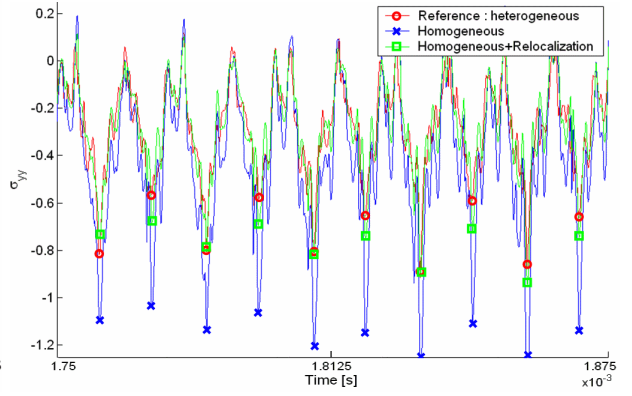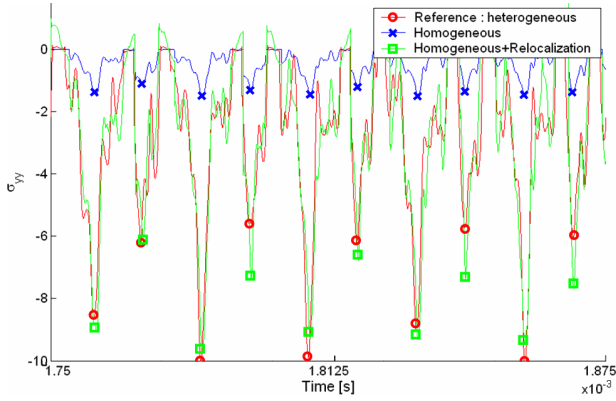

Figure 14. σ_{yy} stress in element A, (figure 3) owing to heterogeneity and in contact with the rigid flat surface, for two calculation processes: direct and with the re-localization process. $P = 0.5MPa$, $\mu = 0.25$, for the heterogeneous model : $\delta = 1500ns$ and for the homogeneous one : $\delta = 1700ns$.

Figure 15. σ_{yy} stress in element B (figure 3), owning to the matrix, for two calculations processes, direct one and with re-localization process. $P = 0.5MPa$, $\mu = 0.25$, for the heterogeneous model : $\delta = 1500ns$ and for the homogeneous one : $\delta = 1700ns$.

(a) Direct calculation.

(b) Re-localization calculation.
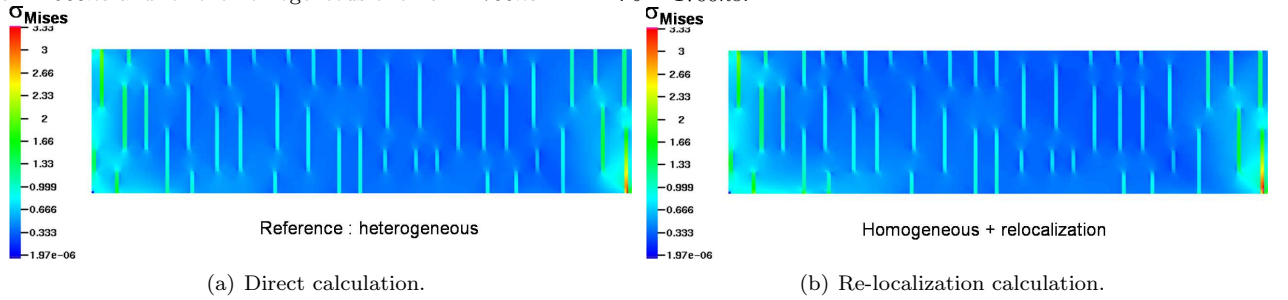
Figure 16. Von Mises stress averaged through time for two calculations processes, direct one and with re-localization process. $P = 0.5$MPa, $\mu = 0.25$, for the heterogeneous model : $\delta = 1500ns$ and for the homogeneous one : $\delta = 1700ns$.

For every element, the results given by the re-localization process (from the homogeneous model), for σ_{yy}, are very close to those obtained by a classical dynamical analysis of a heterogeneous model (less than 4% error). However the re-localization process slightly overestimates the positive stress at the surface of the contact because there is no contact law in the relocalization process (figure 14). For the other stresses, σ_{xx}

and σ_{xy}, correlation is very good when the element studied is in the volume ($< 4\%$) and slightly worse when it is at the surface (up to 25%). The main stress is σ_{yy} and whatever the element studied the values of the mean and the standard deviation given by the re-localization process are very good (differences $< 5\%$).

In conclusion it was shown in this section that the re-localization process is able to give a good approximation of the stresses present in a heterogeneous model and of their evolution through time simply by performing a static calculation of the heterogeneous model and a dynamical contact and friction analysis of an equivalent homogeneous model.

6. CONCLUSION

This paper focused on the numerical study of a composite under non linear dynamical loading. The model and the general problem of convergence of numerical models subjected to dynamic contact with friction loading has been addressed. The use of a regularized friction law makes it possible to achieve good convergence between such models. The main results highlight that homogenization is a means of mapping from mesoscopic to macroscopic scale, provided that the regularization time of the homogeneous model gives it the same mode of instability as the heterogeneous model. Moreover, this study emphasizes the very important role of contact dynamics in friction problems. It has been shown that all heterogeneous models can be represented by homogeneous ones, though it is necessary to adapt the regularization time if the model is very unstable. This modification of regularization time can be considered as a homogenization of local contact dynamics. In fact the latter beneath the heterogeneities is certainly different from the contact dynamics beneath the matrix. Consequently, the regularization time, a dynamic parameter of the friction law, must be different in the heterogeneous model from that in the homogeneous one. A formula based on energy conservation is presented. It allows determining a "homogenized" local friction coefficient in the case where the different constituents of the material have different local friction coefficients. Finally, the mapping from macroscopic to mesoscopic scale is developed by a simple re-localization procedure. Determining the evolution of stresses through time is made possible by simple static calculations of the heterogeneous model and a non linear dynamical analysis of the homogeneous equivalent model.

References

Adams, G.G., 1995. Self-excited oscillations of two elastic half-spaces sliding with a constant coefficient of friction. Journal of Applied Mechanics 62, 867-872.

Alart, P., Lebon F., 1998. Numerical study of a stratified composite coupling homogenization and frictional contact. Mathematical and Computer Modelling 28 (4-8), 273-286.

Baillet, L., Sassi, T., 2002. Finite element method with Lagrange multipliers for contact problems with frictions. Comptes Rendus de l'Académie des Sciences 334, 917-922.

Baillet, L., Linck, V., D'Errico S., Laulagnet, B., Berthier, Y., 2005. Finite element simulation of dynamic instabilities in frictional sliding contact. Journal of Tribology, Trans. ASME, 127, 652-657.

Bathe, K.J., 1982. Finite element procedures in engineering analysis. Prentice-Hall, New-York.

Ben-Zion, Y., 2001. Dynamic ruptures in recent models of earthquake faults. Journal of the Mechanics and Physics of Solids 49, 2209-2244.

Bornert, M., Bretheau, T., Gilormini, P., 2001. Homogénéisation en mécanique des matériaux, Vol.1 - Matériaux aléatoires élastiques et milieux périodiques. Hermès Science.

Boutin, C., 1991. Diffraction rayleigh dans les milieux élastiques hétérogènes. CNRS-Rapport GRECO Géomatériaux Aussois, 101-108.

Boutin, C., Auriault, J.L., 1993. Rayleigh scattering in elastic composite materials. International Journal of Engineering Science 31 (12), 1669-1689.

Boutin, C., 1996. Microstructural effects in elastic composites. International Journal of Solids and Structures 33 (7), 1023-1051.

Chen, W., Fish, J., 2001. A dispersive model for wave propagation in periodic heterogeneous media based on homogenization with multiple spatial and temporal scales. Journal of Applied Mechanics 68 (2), 153-161.

Cochard, A., Rice, J.R. Fault rupture between dissimilar materials: Ill-posedness, regularization and slip-pulse response. Journal of Geophysical Research 105 (25), 891-907.

Fish, J., Chen, W., 2004. Space-time multiscale model for wave propagation in heterogeneous media. Computer Methods in Applied Mechanics and Engineering 193, 4837-4856.

Hughes, T.J.R., 1987. The finite element method - Linear static and dynamic finite element analysis. Prentice-Hall, Englewood Cliffs.

Kanit, T., Forest, S., Galliet, I., Mounoury, V., Jeulin, D., 2003. Determination of the size of the representative volume element for random composites: statistical and numerical approach. International Journal of Solids and Structures 40 (13-14), 3647-3679.

Kruch, S., Forest, S., 1998. Computation of coarse grain structures using a homogeneous equivalent medium. Journal de Physique IV 8, 197-205.

Kruch, S., Feyel, F., Chaboche, J.L., 2004. Application de l'homogénéisation périodique aux structures à gros grains. ONERA

Lemaitre, J., Chaboche, J.L., 2004. Mécanique des matériaux solides. Dunod.

Linck, V., Baillet, L., Berthier, Y., 2003. Modeling the consequences of local kinematics of the first body on friction and on third body sources in wear. WEAR 255, 299-308.

Linck, V., 2005. Temporal numeric modelization of a contact with friction. PhD thesis, INSA-Lyon.

Lykotrafitis, G., Rosakis, A.J., 2004. Sliding of frictionally held incoherent interfaces under dynamic shear loading. In: Proceedings of 2004 ASME/STLE International Joint Tribology Conference.

Martins, J.A.C., Barbarin, S., Raous, M., Pinto Da Costa, A., 1999. Dynamic stability of finite dimensional linearly elastic systems with unilateral contact and Coulomb friction. Computer Methods in Applied Mechanics and Engineering 177, n° 3-4, 289-328.

Martins, J.A.C., Simões, F.M.F., 1998. Instability and ill-posedness in some friction problems. International Journal of Engineering Sciences 36, 1265-1293.

Massi, F., Baillet, L., Giannini, O., Sestieri A., 2007. Brake squeal: linear and nonlinear numerical approaches. Accepted in Mechanical Systems and Signal Processing.

Oueslati, A., Nguyen, Q.S., Baillet, L., 2003. Stick-slip separation waves in unilateral and frictional contact. Comptes Rendus de l'Académie des Sciences 331, 133-140.

Peillex, G., Baillet, L., Berthier, Y., 2006. Comparison between two scales for the modeling of c/C composites under tribological solicitation. In: Proceedings of the ECCM12.

Prakash, V., Clifton, R.J., 1993. Time resolved dynamic friction measurements in pressure-shear. Experimental Techniques in Dynamics of Deformable Solids 165, 33-48.

Prakash, V., 1998. Frictional response of sliding interfaces subjected to time varying normal pressures. Journal of Tribology, Trans. ASME, 120, 97-102.

Ranjith, K., Rice, J.R., 2001. Slip dynamics at an interface between dissimilar materials. Journal of the Mechanics and Physics of Solids 49, 341-361.

Renardy, M., 1992. Ill-posedness at the boundary for elastic solids sliding under coulomb friction. Journal of Elasticity 27, 281-287.

Sanz-Serna, J.M., Spijker, M.N., 1986. Regions of stability, equivalence theorems and the Courant-Friedrichs-Lewy condition. Numerische Mathematik 49, 319-329.

Xia, K., Rosakis, A.J., Kanamori, H., 2004. Spontaneous rupturing along a frictional interface. In: Proceedings of 2004 ASME/STLE International Joint Tribology Conference.

Acknowledgment